iScience, Volume *24*

Supplemental information

Structure basis for AA98 inhibition on the activation of endothelial cells mediated by CD146

Xuehui Chen, Huiwen Yan, Dan Liu, Qingji Xu, Hongxia Duan, Jing Feng, Xiyun Yan, and Can Xie

Supplemental Information

Structure Basis for AA98 Inhibition on the Activation of Endothelial Cells Mediated by CD146

Xuehui Chen, Huiwen Yan, Dan Liu, Qingji Xu, Hongxia Duan, Jing Feng, Xiyun Yan and Can Xie

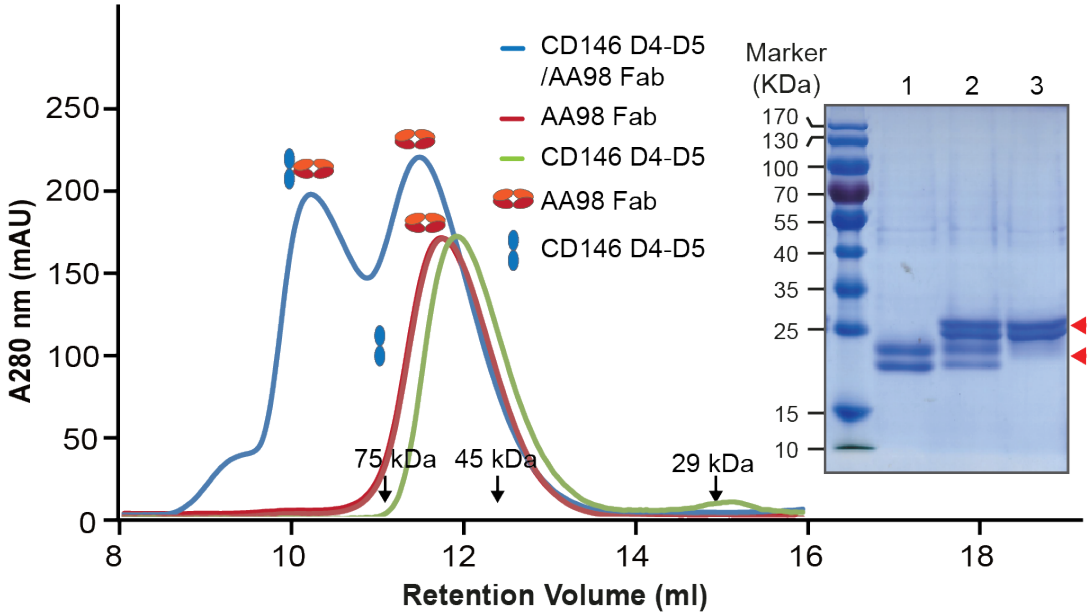

Figure S1. Protein purification of CD146 D4-D5 in complex with AA98 Fab. Related to Figure 1. Size-exclusion chromatography (Superdex 75 10/300 GL) analysis of purified CD146 D4-D5 protein (residues 336-519, green curve), AA98 Fab (red curve), and complex CD146 D4-D5/AA98 Fab protein (blue curve). SDS-PAGE (Inset) shows the purified CD146 D4-D5 from the peak of the green curve (Lane 1), the purified Fab AA98 from the peak of the red curve (Lane 3) and the complex CD146 D4-D5/AA98 Fab protein from the first peak of the blue curve (Lane 2). All eluted fractions were analyzed by 12% SDS–PAGE and stained with Coomassie Brilliant Blue. Black arrows indicate the elution positions for the standard marker in size-exclusion chromatography and red arrows show the position of CD146 D4-D5 protein and AA98 Fab in SDS-PAGE.

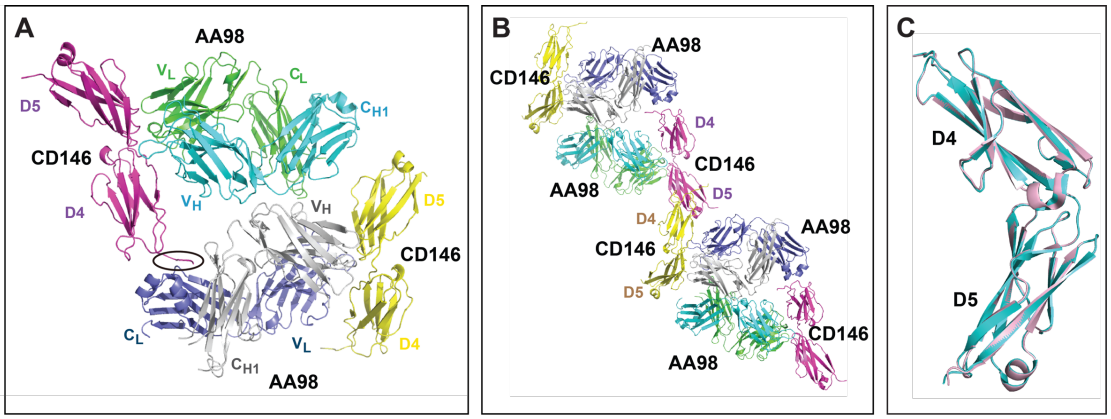

Figure S2. Crystal structure of CD146 D4-D5/AA98 Fab complex in the asymmetric unit. Related to Figure 1. (A) Two CD146 D4-D5/AA98 Fab complexes in the asymmetric unit. **(B)** Ribbon diagram of CD146 D4-D5/AA98 Fab complexes from two adjacent asymmetric unit which have interactions in CD146 part due to crystal packing. In the asymmetric unit, major interactions between different complex are those from AA98 Fab molecules. Apart from this, the extended loop from the remnant of CD146 D3 and D3-D4 linker (residues 337-341, elliptical part in **A**) interacted with the κ chain of another AA98 Fab (as shown in **B**). This is also the same part which interacts with the bottom of D5 from another symmetry related CD146 molecule (as shown in **B**). **(C)** Superposition of CD146 D4-D5 in asymmetric unit. CD146 D4-D5 molecules from asymmetric unit were superposed. One molecule is colored in lightpink while the other in cyan. The r.m.s.d. from the superposition of the CD146 Cα atoms are 0.31 Å. These two molecules are almost identical except for the tail of D5.

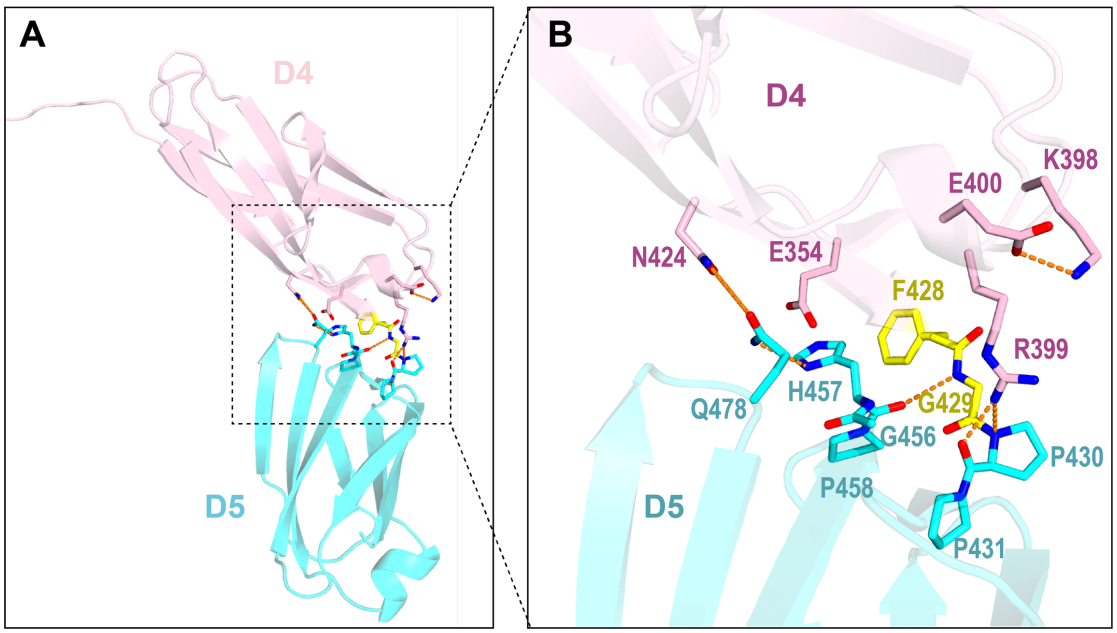

Figure S3. Interface between CD146 D4 and D5. Related to Figure 1. (A) Interface between CD146 D4 and D5 (AA98 Fab omitted for clarity). CD146 D4-D5 are shown in cartoon representation, and residues in D4 is colored in light pink, while those in D5 is colored in cyan. The two residues in the D4-D5 linker are colored in yellow. Residues in the D4-D5 interface are shown in sticks. (B) Enlargement of the residues in the red dashed line box, describing the direct interactions between D4 and D5 in the presence of AA98 Fab (omitted for clarity). Oxygen atoms are colored red and nitrogen atoms are blue. Hydrogen bonds are shown by orange dashed lines. For clarity, some residues and related interactions are omitted. Colors are as described in A.

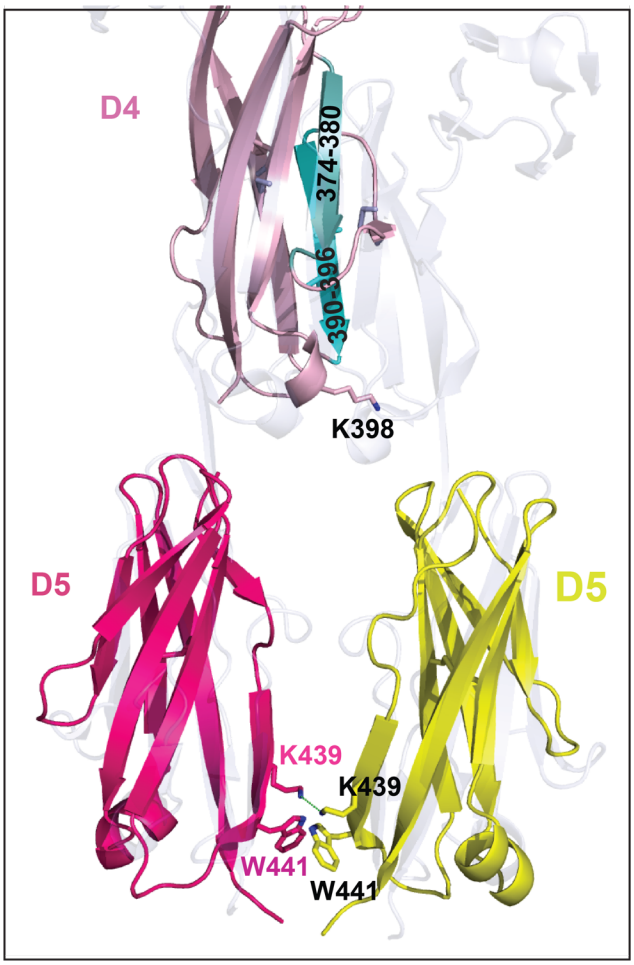

Figure S4. Identification of the potential CD146 dimer interface. Related to Figure 2. Superposition of CD146 D4-D5 on the corresponding domains of the ICAM-1 D3-D5 dimeric form. ICAM-1 D3-D5 is shown as the background and color in lightblue. One molecule of CD146 D4 is shown in lightpink and D5 in hotpink. Another CD146 D5 is superposed on the ICAM-1 dimer D5 and color in yellow. The deleted fragments are labelled. 374E-380E fragment is colored in lighteal while fragment 390P-396D is colored in cyan .The two residues, K398 in CD146 D4 and K439 in CD146 D5, that contribute to the dimerization in the chemical cross-linking test shown in stick representation. The dash line shows the distance between the two K439 from speculative adjacent CD146 D5. Also shown in stick representation are residues W441 in D5.

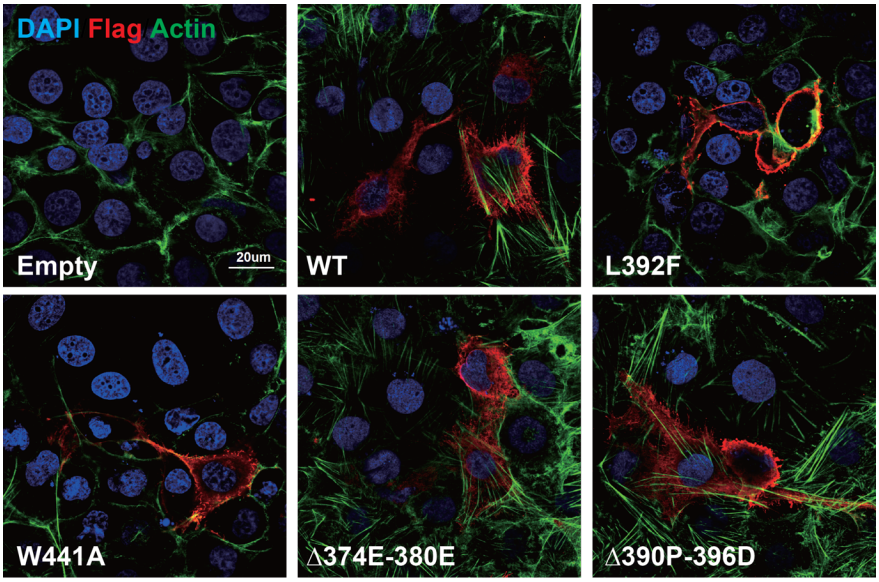

Figure S5. Decreased assembly of F-actin caused by CD146 steady-state. Related to Figure 3. Assembly of F-actin in HUVECS transfected with CD146 wild-type and CD146 mutants. Bar = 20μm.

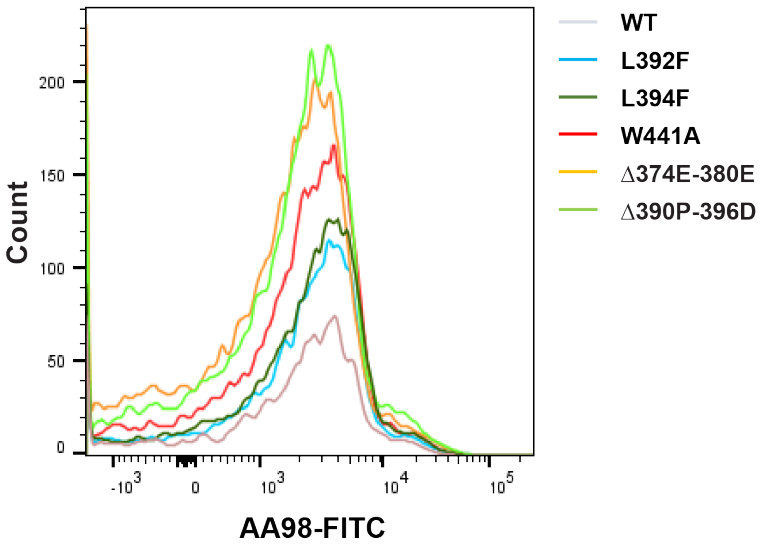

Figure S6. The mutations on CD146 do not affect AA98 binding. Related to Figure 3. 293T cells were transfected with constructs containing CD146 mutations, and AA98 binding affinity to different CD146 mutants were measured with FITC labeled AA98 mAb by FACS.

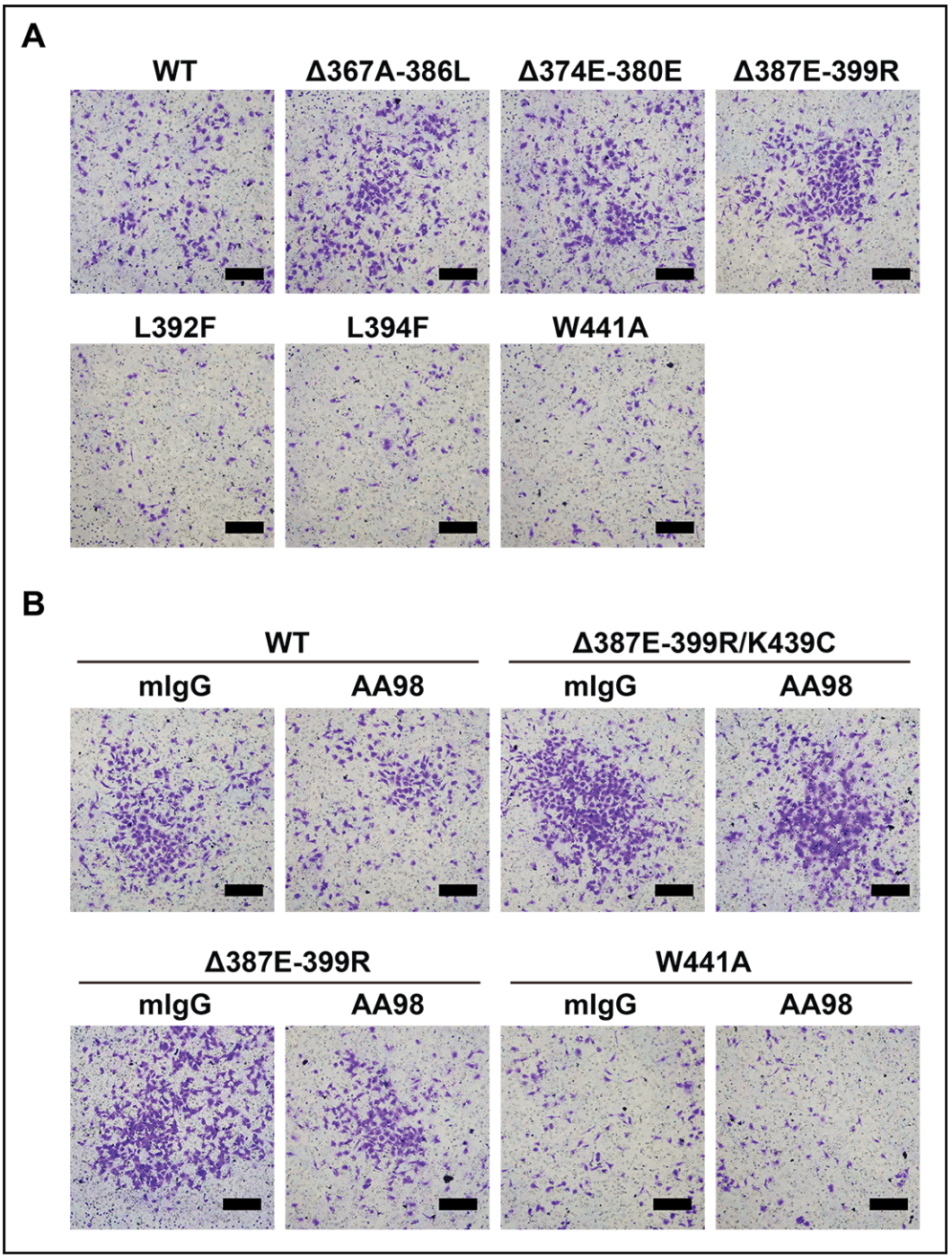

Figure S7. The representative images in the transwell migration assays. Related to Figure 3. (A) HUVECs transfected with different mutant constructs of CD146 were subjected to a transwell migration assay and representative images were shown (related to Figure 3C). **(B)** Transwell assay analysis of the migration activity of mutants transfected with HUVECs treated with AA98 or not and representative images were shown (related to Figure 3F). Bar = 50μm.

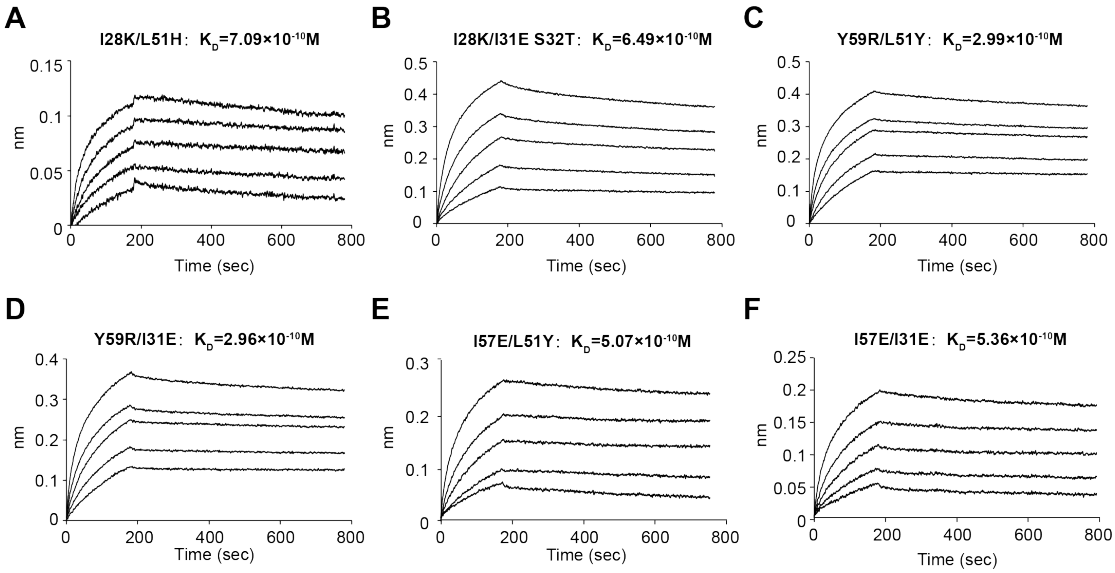

Figure S8. The improved binding affinity of rationally designed AA98 mutants to CD146. Related to Figure 4. BLI-binding assay was used to measure the affinity of a series of AA98 mutations, which were rationally designed to improve the binding affinity to CD146.**A-F** correspond to I28K/L51H, I28K/I31E, Y59R/L51Y, Y59R/I31E, I57E/L51Y, and I57E/I31E, respectively.

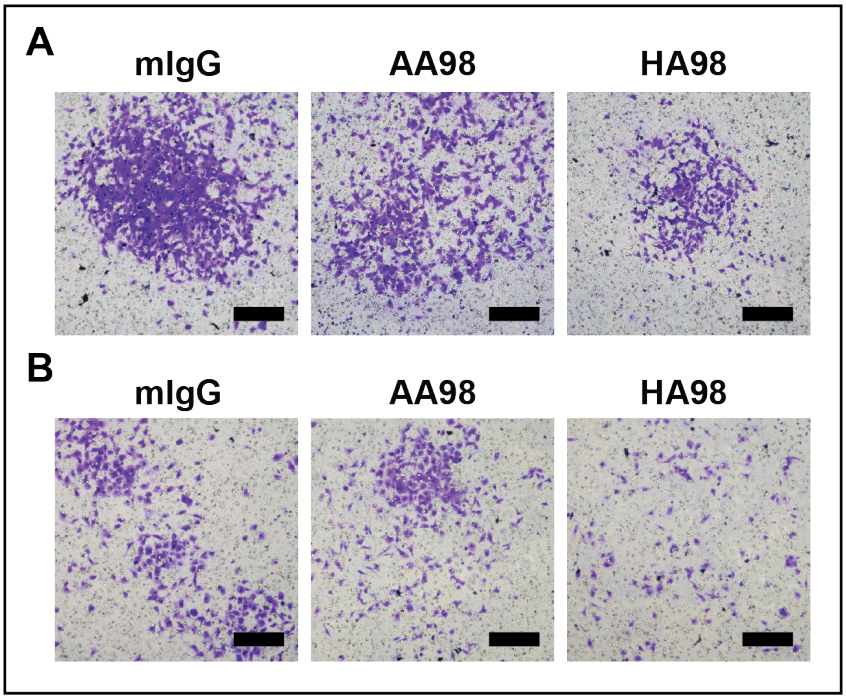

Figure S9. The representative images in the transwell migration assays. Related to Figure 4. MDA-MB-231 **(A)** and HUVECs **(B)** treated with mIgG (control), AA98 and HA98 were subjected to a transwell migration assay and representative images were shown, related to Figure 4F and Figure 4G, respectively. Bar = 50μm.

Transparent Methods

Recombinant Protein Expression and Purification

The construct for the CD146 domain 4-5 fragment (Gln336-Leu519) was inserted into the expression vector pEF1/puro (a vector based on pEF1/V5-HisA modified to contain a puromycin sequence). We added a CD146 signal peptide, followed by a His tag and an SBP tag, to the N-terminus of the fragment. A PreScission protease recognition sequence was introduced between the SBP tag and the CD146 D4-D5 fragment. Recombinant proteins were purified from CHO Lec 3.2.8.1 cell supernatants by affinity chromatography (Ni-NTA followed by strep-tactin column). The purified protein was digested with PreScission protease to remove the fused affinity tag and further deglycosylated with endoglycosidase H. Undigested proteins and protease were removed by reloading onto a Ni-NTA column. The CD146 D4-D5 protein was further purified by Superdex 200(GE Healthcare Life Sciences, Chalfont) gel filtration in 10 mM Tris-HCl, pH 8.0, 0.15 M NaCl.

The AA98 antibody was purified from the culture supernatant with a protein A column followed by Superdex 200 (GE Healthcare Life Sciences, Chalfont) gel filtration. The Fab was generated by immobilized papain (Pierce, Rockford, IL) digestion following the manufacturer's instructions. Undigested IgG and Fc fragments were removed by reloading onto the Protein A column, and the Fab was purified further by Superdex 75 (GE Healthcare Life Sciences, Chalfont) gel filtration in 20 mM HEPES, pH 7.5, 0.15 M NaCl. The purified CD146 D4-D5 fragment was incubated with AA98 Fab at a 1:4 molar ratio on ice for 30 min. The D4-D5 complex with Fab was separated from excess free Fab using Superdex 200 (GE Healthcare Life Sciences, Chalfont) in 10 mM Tris (pH 8.0) and 150 mM NaCl and

concentrated for crystallization.

Crystallization

Crystals were grown by using vapor diffusion in hanging drops at 291 K with equal volumes of 12 mg/ml protein solution and a reservoir solution of 19% PEG2000MME / 50 mM HEPES (pH 7.8). Crystals were cryoprotected by transfer to Ail's oil. The sequence of the AA98 Fab was determined by hybridoma cDNA sequencing exactly as previously described(Chen et al., 2007).

Structure Determination and Refinement

The diffraction data were collected at the 19-ID beamline of the Shanghai Synchrotron radiation Facility (SSRF, China)(Zhang et al., 2019) and processed with the program suite HKL2000(Otwinowski and Minor, 1997). The Phaser program(McCoy et al., 2007) was used for molecular replacement. The model used was the Fab fragment from D2.3 (PDB code1YEC(Charbonnier et al., 1997)). The solutions from molecular replacement were subjected to iterative cycles of model rebuilding in COOT(Emsley et al., 2010) and refinement using Phenix(Adams et al., 2010). After several cycles of refinement, manual model building and refinement for CD146 D4-D5 were performed. Sigma A-weighted 2 Fo-Fc and Fo-Fc maps were computed during the refinement, and refinement was monitored by the decrease in R_{free}. Composite omit maps were calculated during refinement to reduce model bias. The final model, refined to 2.8Å resolution, contains amino acid residues 336–519 of CD146 D4–D5, residues 1–217 of the AA98 Fab light chain, residues 1–132 and 138–217 of the Fab heavy chain, and two carbohydrate residues. Model geometry was verified using the program ProCheck(Laskowski et al., 1993). Solvent molecules were located from stereo

chemically reasonable peaks in the σA-weighted Fo-Fc map. Final refinement statistics are summarized in Table 1. Structural figures were prepared with the program PyMol(DeLano, 2002).

Expression and Purification of AA98 Mutants

Gene sequences of AA98 mutants were cloned into the pEF expression vectors. Various variable regions were subcloned into expression vectors containing the appropriate mouse IgG2a H- and L-chain constant-region sequences by extension PCR. Constructs with different combinations of the light chain and the heavy chain were transiently cotransfected into 293T cells. The conditioned media from the transient production run were harvested and clarified by centrifugation. The supernatants were purified with a Protein A column as described above. Antibodies were further purified by size exclusion chromatography (Superdex 200 Increase 10/300 GL, GE Healthcare).

BLI-binding studies

Purified recombinant CD146 ectodomain was immobilized on Octet red system biosensors (Pall ForteBio, CA, USA). The bound CD146 ectodomain was diluted into kinetics buffer (PBS, pH 7.4, 0.01% (w/v) BSA, 0.002% (v/v) Tween-20) at 10 μg/mL and immobilized onto AMC biosensors (FortéBio). Following a 120 s baseline step, biosensors were dipped into wells containing a two-fold dilution series of AA98 IgG. Sensors were then dipped back into kinetics buffer to monitor the dissociation rate. Kinetics data were analyzed using FortéBio's Data Analysis software 9.0, and kinetic curves were fitted to a 1:1 binding model. The mean kinetic constants reported are the results of three independent experiments.

Cell migration assay

Cell migration was assayed using a modified Boyden chamber assay (8 μm pore size; Costar; Corning) as described previously (Zheng et al., 2009). After the appropriate treatments, cells were trypsinized, washed, and resuspended in fresh serum-free medium (10,000 cells per well). After incubation at 37°C overnight, cells remaining at the upper surface of the membrane were removed using a swab, and cells that had migrated to the lower membrane surface, which are representative of migrated cells, were fixed with 4% paraformaldehyde and stained with Giemsa solution. Pictures were taken on an OLYMPUS BX51 microscope with a UPlanFLN digital camera using a 4/0.13 numeric aperture objective. Cells migrating through the filter were counted and plotted as the number of migrating cells per optic field.

Cell proliferation assay

The cell proliferation assay was conducted using the cell counting kit-8 (HY-K0301, MCE) following the manufacturer's instruction. Briefly, the cells were seeded into a 96-well plate in triplicates at the density of 3000 cells/100 μl. After 48 h, 10 μl dye solution was added and incubated at 37 ℃ for 3-4 h. The absorbance at 450 nm was measured using Mark microplate absorbance reader (Bio-Rad).

Immunofluorescence

Cells were plated on slides cultured in 6-well plates and then subjected to the appropriate treatments. The cells were washed with PBS, fixed in acetone/methanol (1:1) for 30 seconds, permeabilized with 0.1% Triton X-100, blocked with 5% normal goat serum for 60 min at 37°C, and then incubated with phalloidin for 1 hour. Coverslips were subsequently examined with a confocal laser scanning microscope (Olympus FLUOVIEW FV 1000) with an Olympus IX81 digital camera using a 20×/0.75 numeric aperture objective.

Immunohistochemistry

Paraffin-embedded tissue sections were deparaffinized and stained first with an antibody for CD31 and then with HRP-conjugated secondary antibody. The sections were then stained with 3'3-diaminobenzidine(DAB) and finally counterstained with hematoxylin. The length of blood vessels per tumor in each group was quantified by ImagJ software in 10 random areas per section. Images were taken on a OLYMPUS BX51 microscope with a UPlanFL N digital camera using 10×/0.3 numeric aperture objective.

Animal experiments

Female 5-week-old BALB/c nude mice were kept under specific pathogen-free conditions. Xenografts of A375 cell lines were produced by injecting tumor cells (1×10^7 resuspended in PBS) subcutaneously into the backs of mice. When the tumors reached 5-8 mm, the mice were grouped (8 mice per group) and administered purified mAb HA98, AA98 or mIgG at a dose of 150 μg per mouse twice per week by intraperitoneal injection. Tumor size was measured twice per week, and tumor volume was determined according to the following equation: tumor size = $\text{width}^2 \times \text{length} \times (1/2)$.

This study was approved by the Ethical Review Committee of Institute of Biophysics, Chinese Academy of Sciences, China. All methods in this work were performed in accordance with the People's Republic of China regulation of experimental animals.

Statistical analysis

All experiments were done in triplicate. Data were shown as means ± SEM. Statistical differences were determined by One-way ANOVA. $P < 0.05$ was considered stastically significant. The statistical analyses were performed with GraphPad Prism 5.0.

Data deposits

Atomic coordinates and the structure factor files have been deposited in the Protein Data Bank (http://www.rcsb.org) under accession number 6LYN.

References

Adams P.D,, Afonine. P., Bunkóczi G, Chen V.B,, Davis I.W,, Echols N, Headd J.J, Hung L.W., Kapral G.J., Grosse-Kunstleve R.W. et al. (2010). PHENIX: a comprehensive Python-based system for macromolecular structure solution. *Acta Crystallogr D Biol Crystallogr.,* 66**,** 9. 10.1107/S0907444909052925

Charbonnier JB, Golinelli-Pimpaneau B., Gigant B, Tawfik DS, Chap R, Schindler DG, Kim SH, Green BS, Eshhar Z and Knossow M. (1997). Structural convergence in the active sites of a family of catalytic antibodies. *Science,* 275**,** 3. 10.1126/science.275.5303.1140

Chen, X., Kim, T. D., Carman, C. V., Mi, L. Z., Song, G. and Springer, T. A. (2007). Structural plasticity in Ig superfamily domain 4 of ICAM-1 mediates cell surface dimerization. *Proc Natl Acad Sci,* 104**,** 8. 10.1073/pnas.0707406104

DeLano, W. I. (2002). The PyMOL Molecular Graphics System, Version 2.0 Schrodinger, LLC.

Emsley, P., Lohkamp, B., Scott, W. G. and Cowtan, K. (2010). Features and development of Coot. *Acta Crystallogr D Biol Crystallogr,* 66**,** 486-501. 10.1107/S0907444910007493

Laskowski, R., MacArthur, M. W., Moss, D. S., and Thornton, J. M. (1993). PROCHECK: a program to check the stereochemical quality of protein structures. *J. Appl. Cryst,* 26**,** 283-291.

McCoy, A. J., Grosse-Kunstleve, R. W., Adams, P. D., Winn, M. D., Storoni, L. C. and Read, R. J. (2007). Phaser crystallographic software. *J Appl Crystallogr,* 40**,** 658-674. 10.1107/S0021889807021206

Otwinowski Z and Minor. W. (1997). Processing of X-ray diffraction data collected in oscillation mode. *Methods Enzymol. ,* 276**,** 20. 10.1016/S0076-6879(97)76066-X

Zhang, W., Tang, JC., Wang, SS. et al. (2019). The protein complex crystallography beamline (BL19U1) at the Shanghai Synchrotron Radiation Facility. *Nucl Sci Tech,* 30. 10.1007/s41365-019-0683-2

Zheng C, Qiu. Y., Zeng Q, Zhang Y, Lu D, Yang D, Feng J and Yan X. (2009). Endothelial CD146 is required for in vitro tumor-induced angiogenesis: the role of a disulfide bond in signaling and dimerization. *Int J Biochem Cell Biol.,* 41**,** 10. 10.1016/j.biocel.2009.03.014